LTE-based Pervasive Sensing Across Indoor and Outdoor

Yuda Feng
University of Massachusetts Amherst
Amherst, MA, USA
yudafeng@umass.edu

Yaxiong Xie
Princeton University
Princeton, NJ, USA
yaxiongx@princeton.edu

Deepak Ganesan
University of Massachusetts Amherst
Amherst, MA, USA
dganesan@cs.umass.edu

Jie Xiong
University of Massachusetts Amherst
Amherst, MA, USA
jxiong@cs.umass.edu

ABSTRACT

Besides the communication function, wireless signals are recently exploited for sensing purposes, enabling diverse applications. However, designing a wireless sensing system that provides truly pervasive coverage at city or even national scale and at the same time does not affect ongoing data communication is still challenging. In this work, we propose to involve the pervasive LTE signals into the ecosystem of wireless sensing. Although LTE sensing solves the coverage issue and does not compromise the communication function, it brings unique challenges. Due to the long distance between LTE base stations and terminals, the LTE signal interacts with diverse objects during the propagation process which causes severe interference in sensing. We enable LTE sensing by designing delicate signal processing schemes to combat against the severe interference. We demonstrate the advantages of LTE sensing using two typical applications, indoor respiration sensing and outdoor traffic monitoring. Extensive experiments show that the proposed system can achieve highly accurate respiration sensing with the blind spot and orientation-sensitive issues greatly mitigated. For traffic monitoring, the error of car speed estimation is lower than 2 mph, as good as commercial devices on the market.

CCS CONCEPTS

• **Human-centered computing → Ubiquitous and mobile computing systems and tools**.

KEYWORDS

LTE Sensing, Pervasive sensing, Outdoor sensing, Interference

ACM Reference Format:
Yuda Feng, Yaxiong Xie, Deepak Ganesan, and Jie Xiong. 2021. LTE-based Pervasive Sensing Across Indoor and Outdoor. In *The 19th ACM Conference on Embedded Networked Sensor Systems (SenSys'21), November 15–17, 2021, Coimbra, Portugal.* ACM, New York, NY, USA, 14 pages. https://doi.org/10.1145/3485730.3485943

Permission to make digital or hard copies of all or part of this work for personal or classroom use is granted without fee provided that copies are not made or distributed for profit or commercial advantage and that copies bear this notice and the full citation on the first page. Copyrights for components of this work owned by others than ACM must be honored. Abstracting with credit is permitted. To copy otherwise, or republish, to post on servers or to redistribute to lists, requires prior specific permission and/or a fee. Request permissions from permissions@acm.org.
SenSys'21, November 15–17, 2021, Coimbra, Portugal
© 2021 Association for Computing Machinery.
ACM ISBN 978-1-4503-9097-2/21/11…$15.00
https://doi.org/10.1145/3485730.3485943

1 INTRODUCTION

Wireless sensing has become a popular area of research in the last few years. Different from traditional sensor-based sensing, wireless sensing relies on signals reflected from target to obtain the target information. The contact-free nature of wireless sensing is particular appealing in current COVID pandemic. Various wireless technologies have been exploited for sensing including WiFi [25, 33, 47], RFID [45], mmWave [9, 18] and LoRa [42, 43, 48, 49]. Among these technologies, WiFi sensing attracted most attention owning to the pervasive deployment of WiFi access points (APs) in indoor environments. A large variety of WiFi-based sensing applications have been proposed such as gesture recognition [24, 52], respiration monitoring [36, 47, 50], and activity tracking [25, 40].

Though promising, WiFi signals cover the indoor-only environment which is just a small portion of the whole area. Furthermore, we observe that even inside a university building with densely deployed WiFi APs, the coverage is still not enough for sensing purposes. This is because WiFi APs are deployed for communication and there is a huge gap between the *communication coverage* and *sensing coverage*. While both light-of-sight (LoS) signal and reflection signals can be used for communication, only weak reflection signals from the target contain the sensing information. Therefore, while the WiFi communication range in indoor environment can reach 30-50 m, the state-of-the-art sensing range is merely 5-10 m [40, 47]. Therefore, even in indoor environment, the deployed WiFi infrastructure is only able to cover a small portion of area for sensing. In a typical house, one WiFi AP can usually cover the whole house for communication but can only cover one or two rooms close to the AP for sensing. From our empirical studies, only 15% of the area in a typical university building is covered in WiFi sensing range.

Another practical issue which was not paid much attention to is that WiFi sensing can greatly affect WiFi data communication. The uncontrolled WiFi data packets are not suitable for sensing due to the random time interval between adjacent packets and frequent packet loss. On the other hand, WiFi beacons are uniformly distributed in time but the beacon frequency (10 Hz) is not high enough for a lot of sensing applications. Therefore, existing WiFi sensing systems need to fully control the WiFi device to transmit dedicated dumb packets at a high frequency (100-250 Hz) to support sensing applications such as gesture recognition [2, 35] and gait recognition [20, 37]. This dedicated packet transmission greatly affects the primary communication function of WiFi.

The third issue with WiFi sensing is that the sensing performance is highly sensitive to target location and orientation. This is a major limitation that hinders the adoption of WiFi sensing in real world. Take respiration sensing as one example, the sensing performance can severely degrade when a target slightly moves or changes the orientation. The location-dependency results in blind spot issue in wireless sensing [50].

Given the issues above, our conclusion is that *while WiFi is pervasive for communication in indoor environments, it is not pervasive for sensing. WiFi sensing also affects communication and the sensing performance is not stable.*

In this work, we ask this question: can we achieve truly pervasive and reliable sensing without compromising data communication? Instead of using WiFi signals for sensing, we propose to exploit LTE signals to achieve the above objectives. We introduce the unique features of LTE signals and the advantages of exploiting LTE signals for sensing below.

- **Pervasive coverage**. LTE base stations are deployed nationwide, and LTE signals cover not just indoor but also outdoor environments. According to the official communication market report of the USA in 2020 [11], 98% of the population and 84% of area are covered by LTE networks.
- **Frequency diversity and spatial diversity**. LTE signals occupy a large frequency range from 400 MHz to 6 GHz with more than 30 frequency bands. In comparison, WiFi APs operate mainly on two narrow bands located at 2.4 GHz and 5 GHz. Also, LTE base stations are delicately deployed to form hexagonal tiling so that there are usually multiple LTE base stations distributed around a user [17]. In our experiments, more than 15 base stations with different frequencies can be detected in our university located in a suburb area.
- **Everlasting high-rate uniform frames**. Different from contention-based CSMA/CA protocol for WiFi, LTE transmissions are precisely organized among adjacent LTE base stations in both time and frequency domains. LTE frames are uniformly distributed in time domain. Even when there is no data transmission going on, the everlasting broadcasted reference subframes (similar to WiFi beacons) can achieve a frequency of 1000 Hz which is much higher than the frequency of WiFi beacons (10 Hz). Therefore, there is no need to transmit dedicated frames for sensing which affect data communication.

These unique features bring LTE advantages over WiFi and other signals for sensing. The national coverage of LTE signals enables ubiquitous sensing across both indoor and outdoor environments. The frequency and spatial diversities help combat against the well-known blind spot issue and orientation-sensitive issue in WiFi sensing. The uniform frame transmission is essentially ideal for sensing purposes. The high frequency broadcasting of reference frames enables LTE to sense high speed movements which is previously challenging for WiFi sensing. Without a need of transmitting any dedicated frames for sensing, the communication function is not affected, which is critical for real-life adoption of wireless sensing.

Inspired by the unique features of LTE signals, we propose LTE-Track, a new sensing modality leveraging LTE signals to realize truly pervasive sensing. We demonstrate the powerful sensing capability of LTE with two typical applications, indoor respiration sensing and outdoor traffic monitoring.

Respiration sensing is an example of fine-grained activity sensing. The chest displacement during the respiration process is around 0.5 cm [50]. For respiration sensing, we resolve the orientation-sensitive issue and blind spot issue by utilizing the frequency and spatial diversities of LTE signals. Traffic monitoring is an example of high-speed movement tracking. Due to the low packet frequency, WiFi signals have difficulties to accurately track movements with a speed larger than 5 m/s. We show that with the high frame frequency of LTE, we can track a car moving at 50 mph (i.e., 22 m/s, 15x faster than human walking). We show that LTE signals can be used to count the number of cars passing by and also the car speed.

Though promising, challenges need to be tackled before we can turn our idea into a functional system. Due to the long propagation distance (200 m to 10 km) from the LTE base station to the LTE terminal, the signal-to-noise-ratio (SNR) of the received signals is usually 25 - 40 dB lower compared with that of WiFi signals. Therefore, the signal variation induced by target movements can be easily buried in noise. Also, due to the long propagation path, there is more interference during the signal propagation process from moving objects such as swinging trees, moving cars and pedestrians. To mitigate the effect caused by the interference, we propose signal processing methods consisting of coordinate shifting and multi-base-station combining. Leveraging delicate signal processing, we enable accurate respiration sensing and car speed measurement using free signals from LTE base stations.

We summarize the main contributions of this work as follows:

- We effectively utilize the unique features of LTE to address several fundamental issues associated with existing wireless sensing systems. We believe LTE sensing moves one step towards truly pervasive sensing.
- We propose delicate signal processing schemes to combat against severe interference, making LTE sensing possible.
- We demonstrate the unique advantages of LTE sensing using two typical applications, respiration sensing and traffic monitoring. Extensive experiments show that the proposed system can achieve accurate respiration sensing with the blind spot and orientation-sensitive issues greatly mitigated. For traffic monitoring, the car speed estimation error is lower than 2 mph, as good as commercial devices on the market.

The rest of this paper is organized as follows. Section 2 introduces the preliminary knowledge related to LTE sensing. Section 3 explains the unique advantages of LTE sensing in detail. Section 4 presents the challenges and signal preprocessing steps. Section 5 and 6 present the design of two sensing applications. Section 7 presents the hardware implementation and detailed evaluation for both applications. Section 8 surveys the related work. Section 9 discusses the limitations followed by a conclusion in Section 10.

2 LTE PRELIMINARY

In this section, we introduce the background knowledge of LTE protocol and the CSI measurements related to sensing. There are two types of LTE physical layer modes, *i.e.,* frequency division duplexing (FDD) mode and time division duplexing (TDD) mode.

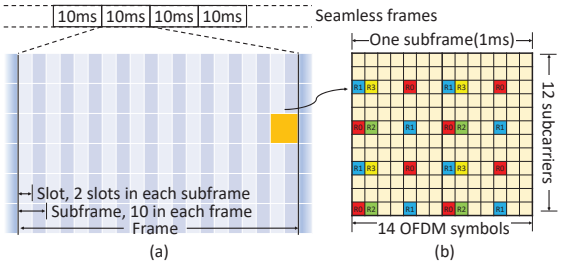

Figure 1: (**a**) The time-frequency resource grids in LTE physical-layer. (**b**) One resource block contains 14 OFDM symbols in time and 12 subcarriers in frequency. The four colors represent the reference signals transmitted by four transmitter antennas.

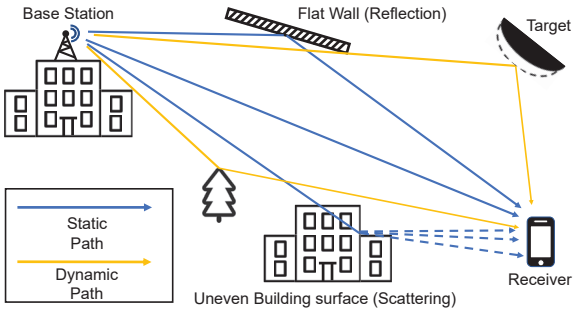

Figure 2: Multiple propagation paths from the transmitter (LTE tower) to the receiver (LTE terminal). The yellow line reflected from the tree represents dynamic path caused by swinging.

We focus on FDD in our design since it is the most widely adopted mode in commercial LTE networks.

2.1 LTE physical-layer frame structure

As shown in Figure 1 (a), LTE physical layer is based on frame structure, which is divided into 10-millisecond *frame*s in the time domain. Each frame is further divided into one-millisecond *subframes*. Each subframe contains 14 OFDM symbols. LTE groups the 14 OFDM symbols (time domain) and 12 subcarriers (frequency domain) into a basic time-frequency unit named *resource block (RB)*, as shown in Figure 1 (b).

2.2 Channel measurement in cellular network

LTE transceivers utilize channel state information (CSI) measurement to reverse the impact of propagation channel for frame decoding. To facilitate channel estimation, LTE base station transmits pre-defined *reference signals*. An LTE terminal is able to estimate the channel using the received reference signal. Specifically, if we use $X(s,f)$ to represent the transmitted known reference signal, and $Y(s,f)$ to represent the received reference signal at the s-th OFDM symbol and f-th subcarrier, the CSI $H(s,f)$ can be calculated as:

$$H(s,f) = \frac{Y(s,f)}{X(s,f)} = \sum_{l=1}^{L} \alpha_l \exp(-j2\pi \frac{d_l}{\lambda}) + n(s,f) \qquad (1)$$

where α_l denotes the complex attenuation, d_l denotes the length of the l-th signal path, L is the number of paths, λ is the wavelength of the signal, and $n(s,f)$ denotes noise. In Figure 1 (b), we show the distribution of reference signals inside each resource block, with four different colors (red, blue, green and yellow) representing four transmitting antennas at the base station. The terminal first estimates the channel of the s-th OFDM symbol and f-th subcarrier that contains reference signal and then interpolates across time and frequency to obtain the full CSI matrix.

3 ADVANTAGES OF LTE SENSING

In this section, we explain the unique advantages of sensing using LTE signals in detail.

Pervasive coverage. The broad coverage of deployed LTE infrastructure provides a sensing coverage that none of the current technologies, including WiFi, Bluetooth and LoRa, can possibly achieve, and thus opens a new window for designing seamless sensing applications at city or even national scale.

Free access. Reference signal is broadcasted by the base station twenty-four seven and receiver device can passively listen and decode the reference signal transmitted from an arbitrary base station. Since decoding the reference signal requires no handshake with the base station, there is no need to purchase a data plan for LTE sensing. In a word, the broadcasted LTE reference signals are free resources available for sensing.

Well-organized and high-frequency channel sampling. As illustrated in Figure 1 (a), the LTE frames and subframes are well-organized without any interframe gap. Therefore, the corresponding CSIs of two consecutive subframes have a strict one millisecond interval in between. Such well-organized uniform sampling is ideal for discrete signal processing. Without dedicated control, other wireless techniques such as WiFi which uses CSMA/CA and LoRa which uses ALOHA, cannot guarantee uniform sampling. Such non-uniform sampling results in either complicated signal processing design or severe degraded sensing performance if blindly assuming uniform sampling.

Another unique advantage is the very high frequency of CSI sampling. If we sample each subframe once, we can obtain 1000 CSI readings per second. This high frequency is critical for applications involving movements of high speed (e.g., car tracking) or high frequency (e.g., motor vibration sensing).

Does not affect on-ongoing data communication. As shown in Figure 1 (b), the time-frequency slots that contain the reference signals are reserved by the cellular protocol so transmitting reference signals do not affect the normal data transmission. On the other hand, sensing using WiFi or LoRa signals usually requires dedicated packets to be transmitted, which occupies the air-time for normal data transmission and affects the overall network throughput.

Frequency and spatial diversity. LTE infrastructure provides rich frequency and spatial diversities, which could be harnessed to improve sensing performance. On the one hand, a single base station supports a large coverage ranging from 200 m (in urban areas) to 10 km (in rural areas) [14]. The placements of LTE base stations are also carefully optimized by the cellular service providers to maximize the signal coverage. Therefore, one mobile device could overhear multiple base stations deployed at diverse locations. According to our experiment results, we are able to detect 15 base

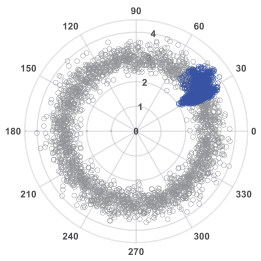

Figure 3: Phase distribution before (grey) and after (blue) random phase offset removal.

stations inside our university. The diverse locations of the overheard base stations provide spatial diversity. Combining the sensing information from various operating frequencies (e.g., 739 Hz,1937.5 Hz and 2115 Hz), the orientation-sensitive and blind spot issues in wireless sensing can be mitigated.

4 SIGNAL PREPROCESSING

While there are numerous advantages for LTE sensing, there are challenges we need to tackle before we can make LTE sensing happen. In this section we introduce the challenges and present the corresponding approaches to address these challenges.

4.1 Challenges

We observe three major challenges when exploiting LTE signals for sensing tasks, which are summarized below:

- **Random phase offsets.** The lack of synchronization between LTE base stations and the terminal results in random phase offsets including carrier frequency offset (CFO), sampling frequency offset (SFO) and sampling timing offset (STO), corrupting the phase information which is critical for sensing.
- **Interference from faraway moving objects.** As the base station could be kilometers away, the signal arriving at the LTE receiver interacts with diverse moving objects along the propagation path shown in Figure 2, such as swinging trees, moving cars and pedestrians. Such interactions cause severe dynamic interference on the received signal.
- **Slow fading.** Slow fading [12] happens when a large obstruction such as a hill or a large building obscures the main signal path between the transceivers, which is quite common for LTE signals. Slow fading causes signal fluctuations that fall into the same frequency range of our daily activities, such as human respiration.

4.2 Signal processing step by step

We present three corresponding signal processing schemes to address the above challenges step by step.

4.2.1 Random phase offset removal. To obtain stable phase for sensing, we need to eliminate the phase offsets caused by CFO, SFO and STO. To facilitate reception diversity, LTE receivers usually have two radio chains connected with two antennas. Since these radio chains share the same oscillator, the random phase offsets are the same at these two radio chains [47]. By conducting a division

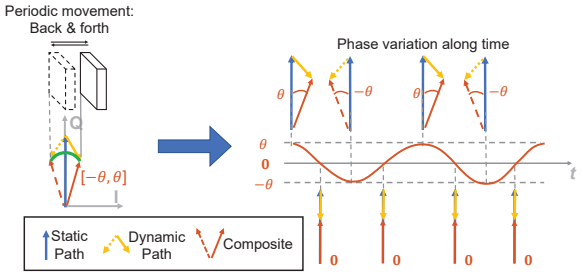

Figure 4: Phase variation induced by periodic movements. By adding the static path signal (blue) and the dynamic path signal (target movement, orange) together, we obtain the composite signal (red). The time series of phase variations form a sinusoidal-like pattern, matching the periodic target movement.

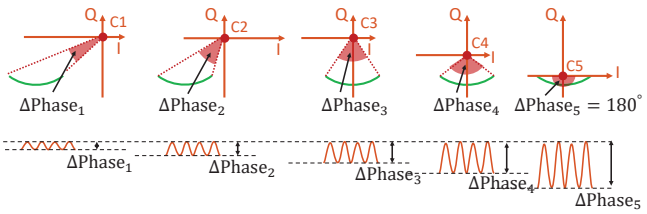

Figure 5: The amount of signal phase variation differs with coordinates.

operation between the complex CSIs from the two antennas, we are able to cancel the common random phase offsets and obtain a stable *phase difference* for sensing. Figure 3 shows the effect of random phase removal, where the grey circles represent the phase readings of the original CSI from one antenna. We can see that random phase offsets cause phase drift in all directions, *i.e.,* all 360°. After random phase offset removal, we obtain stable *phase difference* (blue circles) between two antennas, which falls into a small range of about 25°.

4.2.2 Interference mitigation. After random phase offset removal, we retrieve stable phase readings and thus clean CSI in the I-Q plane. CSI consists of information from signal paths including both static paths and dynamic paths [38]. Figure 4 shows the case with one dynamic path reflected from the target and one combined static path. The phase variation in $[-\theta, \theta]$ forms a sinusoidal-like pattern along time. This matches the periodic target movement and we can then extract the movement information from the signal phase variation. In reality, sensing using LTE signals suffers from interference reflection from other moving objects. We propose a signal processing scheme named heuristic coordinate shifting to mitigate the dynamic interference from other reflectors.

Key intuition. The key intuition of our solution is that the amount of phase variation varies with different coordinates. Therefore, by searching the optimal coordinate, we can amplify the phase variation induced by the target and at the same time suppress the phase variation induced by other interfering reflectors. We use an example in Figure 5 to illustrate this concept. The green arc represents the variation of the complex composite signal in the I-Q plane. It is interesting to see that the phase variations observed from different coordinates (C_1 - C_5) are dramatically different. The small phase variation in C_1 is increased to 180° in C_5.

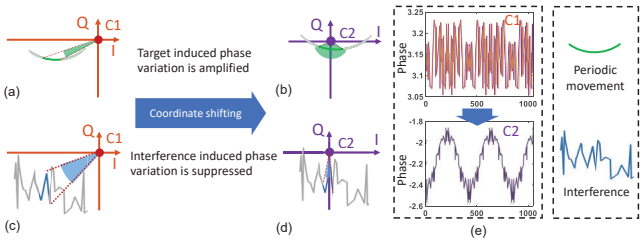

Figure 6: Amplifying target-induced phase variation and suppressing interference-induced phase variation through coordinate change.

We now explain how we address the interference. As shown in Figure 6, we visualize the phase variation induced by target and interference respectively in two coordinates C_1 (orange) and C_2 (purple). We can see that, the target-induced phase variation is significantly increased when we change the coordinate from C_1 to C_2. On the other hand, the interference-induced phase variation is decreased.

Heuristic coordinate shifting. Based on the above intuition, we search for the optimal coordinate that can maximize the phase variation introduced by the target.

To maximize the phase variation, another important property we leverage is that phase variation induced by a lot of applications is periodic. Periodic movement such as respiration obviously induces periodic phase variations. The car movement also induces near-periodic phase variations. This is because within a short time window (e.g., 0.2 s), the car speed can be assumed as constant. Due to the high speed of car, the signal phase varies for multiple cycles within the short time window and the phase variation shows rough periodicity. When the interference is smaller, the phase variation pattern and accordingly the periodicity is clearer as shown in Figure 6(e). Based on the property of periodicity, we search for the optimal coordinate that can maximize the self-correlation of the observed phase variation. For a time window with N complex signal samples $\{(x_1, y_1), (x_2, y_2), ..., (x_N, y_N)\}$, the self-correlation of the phase variation is calculated as:

$$R_\tau = \frac{1}{N-\tau} \frac{\sum_{k=1}^{N-\tau} \theta_k \theta_{k+\tau}}{\pi^2} \tag{2}$$

where θ_k is the phase value of sample (x_k, y_k) and τ is the time lag of the self-correlation. The phase value θ_k depends on the chosen coordinate:

$$\theta_k = \arctan(x_k - O_x, y_k - O_y) \tag{3}$$

where (O_x, O_y) is the origin of the coordinate. Combining Eq. 2 and Eq. 3, we derive our final objective function $R_\tau(O_x, O_y)$ and the optimization problem we are solving is given by:

$$\arg\max_{O_x, O_y, \tau} R_\tau(O_x, O_y) \tag{4}$$

The optimization problem described in Eq. 4 is a constrained nonlinear objective function with the coordinate origin (O_x, O_y) and the time lag τ as the variables. We employ the iterative gradient descend algorithm [13] to solve it. Evaluation of heuristic searching is presented in Section 7.2.1.

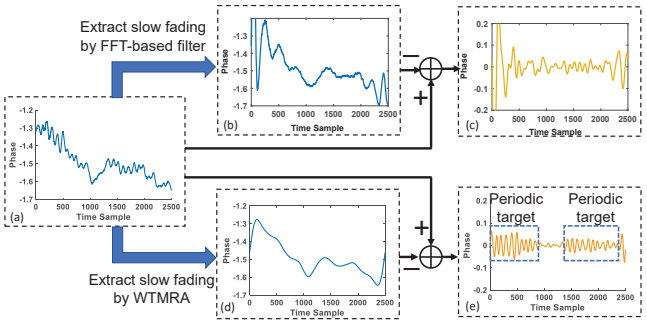

Figure 7: Comparison between FFT-base filter and the proposed WTMRA scheme. (a) Phase variation after coordinate shifting and smoothing. (b) Slow fading extracted by FFT-based filter. (c) Extracted target movement information after slow fading removal using FFT-based filter. (d) Slow fading extracted by the proposed WTMRA scheme. (e) Extracted target movement information after slow fading removal using WTMRA.

We need to adjust several hyper-parameters based on the sensing application. The first parameter we need to adjust is the length of the observation window. With a larger window, we have a larger number of phase cycles[1] for correlation calculation, and accordingly more accurate searching results. However, a larger window also brings a higher computational overhead. Therefore, we adjust the length of the observation window based on application. For a larger target speed which induces a much shorter phase cycle, we reduce the length of the observation window accordingly. For example, the length of the observation window is set to 12 seconds for respiration monitoring and 0.2 second for car speed measurement.

The searching range of time lag τ can also be constrained to reduce the amount of computation. For respiration, the range of human respiration rate is in the range of 10 bpm to 37 bpm [47]. Therefore, we set the search range of τ as $[\frac{60}{37} \times 50, \frac{60}{10} \times 50]$, where $\frac{60}{10} \times 50$ indicates the time lag in terms of number of samples for 10 bpm respiration rate at a sampling rate of 50 Hz.

4.2.3 Residual noise removal. After mitigating the effect of interference, we still need to deal with large-scale signal variation induced by slow fading [12]. Slow fading is caused by large obstructions such as buildings or hills and therefore it is not a problem for WiFi sensing. For LTE signals, because of the long-distance propagation, slow fading is usually noticeable and the slow fading induced variation can sometimes be larger than the variation induced by target movements, degrading the sensing performance. We also observe that the frequency of slow fading is rather close to the frequency of the target movements in frequency domain. Conventional FFT-based filtering methods thus perform poorly to remove the slow fading. Figure 7 (c) shows the result after bandpass filtering in the range of $[0.16\ Hz - 0.62\ Hz]$ (corresponding to 10 bpm to 37 bpm for respiration rate). We can see that there is still residual slow fading left and the periodic signal variation pattern is still distorted.

To better remove the low-frequency slow-fading induced signal variation, we leverage the wavelet-based multiresolution analysis (WTMRA) [7] algorithm, which is a type of filter specialized

[1] One phase cycle corresponds to 360°.

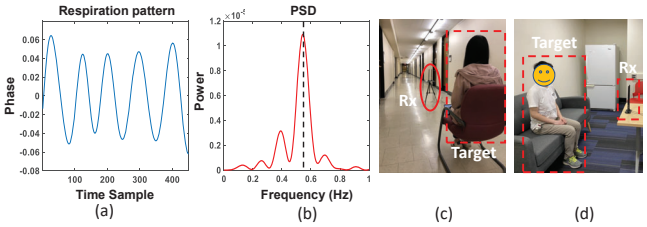

Figure 8: Respiration rate estimation and experiment setting. (a) Respiration pattern obtained after signal preprocessing. (b) FFT of respiration pattern. The peak location represents of respiration rate. (c) A corridor area in the office building. (d) An office room blocked by three walls from the outdoor in the office building.

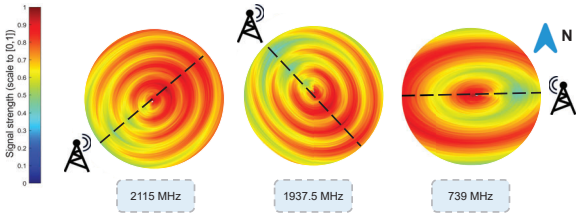

Figure 9: Reflected signal strength distribution around an LTE terminal for 2115 MHz, 1937.5 MHz, 739 MHz base stations, respectively. The three base stations are located in different directions. Combining information from multiple base stations enhance respiration sensing performance.

for low frequency component extraction. One key difference between WTMRA and FFT-based filter is that WTMRA has a higher resolution in low frequency part and therefore can perform more fine-grained filtering in the frequency region of human activities and slow fading.

In detail, WTMRA decomposes the original signal with slow fading into multiple components from the highest Nyquist frequency (half the sampling rate) to low frequency. We set the maximum number of components to be ten, which is enough for both respiration sensing and car speed estimation. We remove the components successively from low frequency to high frequency, and calculate the self-correlation of the remaining signal. We output the remaining signal with the highest self-correlation. Comparing the corresponding results of WTMRA and FFT-based filtering shown in Figure 7, we can see that WTMRA better separates the slow fading, and helps extract cleaner target-induced signal variation pattern.

5 RESPIRATION SENSING

After signal preprocessing, the effect of interference and noise is mitigated. In this section, we present the issues associated with existing respiration monitoring based on wireless sensing and propose methods to address these issues leveraging the unique advantages of LTE signals.

5.1 Respiration rate estimation

To extract the respiration rate, we apply FFT operation on the time-domain signal variation as shown in Figure 8 (a), and then take the peak frequency f_0 to calculate the respiration rate as:

$$R(rpm) = 60 \times f_0 \tag{5}$$

where rpm represents respiration per minute.

5.2 Robustness issues

There are two major robustness issues in existing wireless sensing: the blind spot issue and the target orientation-sensitive issue. In this section, we briefly introduce these two issues and then study their impacts on LTE-based respiration sensing.

Blind spot issue. Blind spot appears because of multipath. Depending on the phase difference, two signals from two propagation paths may superimpose constructively or destructively. Locations where signals superimpose destructively, become blind spots for sensing tasks because of the low SNR of the received signal.

Orientation-sensitive issue. Orientation-sensitive is another issue that compromises the robustness of wireless sensing [36, 47, 50]. When the signal is reflected from the human back but not the front chest, the induced signal variation is much weaker due to a much smaller back displacement during the respiration process.

Impacts on LTE-based respiration sensing. We conduct an experiment to verify the existence of the blind spot issue and orientation-sensitive issue in LTE-base sensing. In this experiment, we measure the strength of signals reflected off a target at locations near an LTE terminal. We repeat the experiment for base stations with a central frequency of 2115 MHz, 1937.5 MHz and 739 MHz. The measured signal strengths are plot in Figure 9, from which we have three observations. First of all, the signal strength shows alternating *peak-valley* patterns along the signal radial direction, and the blind spots for LTE-based sensing locate in the valley area. Second, the peak-valley pattern is an ellipse and the orientation of the ellipse depends on the location of the base station. Third, the width of the peak and valley region depends on the central frequency, *i.e.*, the lower the frequency, the wider peak or valley regions.

We see from Figure 9 that the blind spots still exist in LTE-based sensing. However, different from the blind spots where almost no power can be observed in WiFi sensing [36], the signal strength of the valleys in Figure 9 still maintains at a reasonable high level. Furthermore, since the base stations are distributed in different directions, the orientations of the ellipses are also different, so the blind spots for one base station are highly unlikely still blind spots for another base station. The orientation issue still exists since the signal strength pattern is still an ellipse just like the Fresnel zones [50] in WiFi. If we combine the signal strength pattern of multiple base stations, the target is much less likely to be in the valley regions of all the ellipses.

Takeaway: Blind sport issue and orientation-sensitive issue still exist in LTE sensing. However, these issues can be well mitigated via fully exploiting the spatial and frequency diversities provided by the distributed base stations.

5.3 LTE-based respiration sensing using measurements from multiple base stations

The large number of deployed LTE base stations provide an opportunity to realize truly perverse respiration sensing that can cover both

residential house and large commercial buildings. What is more, the frequency and spatial diversity of LTE base stations can help improve system robustness. We, therefore, propose a scheme that combines the channel measurements from multiple base stations to achieve pervasive and robust respiration sensing.

Combining information from multiple base stations. Each base station has a unique *cell identifier*, which is encoded into the synchronization sequence [21]. Each LTE terminal is able to acquire the cell identifier in the initial stage of synchronizing with the base stations. Equally combining channel measurements from all base stations may not improve the sensing performance as those *bad* respiration patterns cause large errors. We need to assign *high-quality* respiration patterns with larger weights in the combination. Therefore, the problem is how to define a *high-quality* respiration pattern? LTE communication mainly relies on the signal strength or SNR to quantify the signal quality. However, they are not designed for sensing and the sensing performance can not be fully quantified by these metrics. We therefore define a new metric to quantify the respiration sensing quality of LTE signals and we name it RSNR (Respiration SNR).

After signal prepossessing, we obtain the respiration patterns from different base stations. There are always some residual frequency components besides the respiration frequency, as shown in Figure 8 (b). We calculate the ratio between the peak frequency bin's power and the overall power as RSNR. We combine the extracted respiration patterns from multiple base stations using the obtained RSNRs as the weights. The final respiration sensing rate is calculated as:

$$R = \frac{\sum RSNR_i \times R_{LB_i}}{\sum RSNR_i} \tag{6}$$

where $RSNR_i$ denotes the respiration SNR of base station i, and R_{LB_i} denotes the respiration rate obtained from base station i using Equation 5. We empirically remove those base stations with SNR lower than 6 dB, which contribute little to the respiration rate estimation. By combining information from multiple base stations, the amount of blind spots can be significantly reduced as demonstrated in Section 7.2.3.

6 SENSING HIGH SPEED CAR MOVEMENT

Sensing high speed movement in outdoor environments is an essential component of pervasive sensing. To demonstrate the effectiveness of high-speed movement sensing, we build an LTE-based car speed estimation and car counting system.

Car speed estimation and car counting are fundamental services required by many applications for urban traffic monitoring and smart city scheduling. Existing commercial technologies are mainly based on cameras, radar and lidar. Camera-based approaches are affected by illumination, wind, occlusions, etc. Radar and lidar-based car speed estimation devices are usually expensive and require calibration [8] to work properly. By leveraging the advantages of LTE signals, for the first time, we propose an LTE-based passive car movement sensing system that is capable of performing both car speed estimation and car counting.

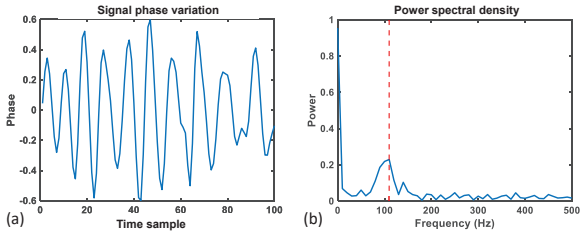

Figure 10: Results of car speed estimation. (a) Phase variation extracted after signal preprocessing. (b) FFT operation on the extracted phase variation, and choose the first peak (not 0 Hz) on the spectrum as the Doppler frequency shift.

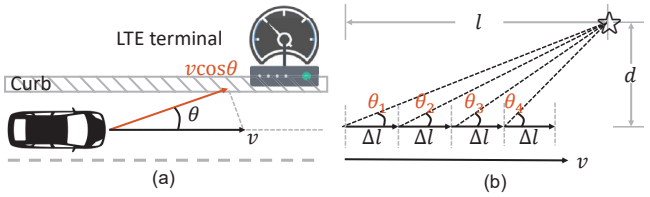

Figure 11: Car speed estimation setup. (a) Diagram of car speed estimation. LTE terminal is placed on the curb of the road. (b) The geometry model used for car speed estimation.

6.1 Car speed estimation

Car movements induce Doppler frequency shift at the signal reflected from the car. We therefore leverage this Doppler shift to estimate the car speed. By applying the signal preprocessing schemes introduced in Section 4, we are able to retrieve clean signal phase variations induced by car movements as shown in Figure 10 (a). This phase variation can be further utilized to obtain the Doppler shift in Figure 10 (b) for speed estimation.

Car detection. Before we estimate the car speed, we need to detect the existence of a car that is approaching or leaving the LTE terminal. Since the car movement causes periodic phase variations as shown in Figure 10 (a), we leverage the window-based self-correlation introduced in Section 4.2 to detect the existence of a moving car. We set the window size as 0.2 second with a 0.1 second overlap between adjacent windows, which is enough to detect at least five cycle of phase variation caused by a car moving at 20 mph. When a peak value greater than five times the other peaks is observed, a moving car is detected.

Speed estimation. We first model the relationship between the car speed and Doppler shift. The root cause of Doppler shift is the change in the length of the signal propagation path [28]. When the path length of the reflection signal changes one wavelength, the phase rotates for a cycle [47]. Supposing the car is moving along the road at a speed of v and the LTE terminal is placed on the curb of a road, then we have $v\cos(\theta)T = \lambda$, where T is the time period required to change the path length by one wavelength λ. Thus, the Doppler shift f_s induced by the car movement to the signal received at the LTE terminal can be calculated as:

$$f_s = \frac{1}{T} = \frac{v}{\lambda}\cos(\theta) \tag{7}$$

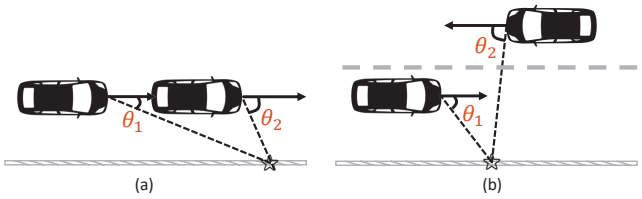

Figure 12: (a) Two cars pass by at the same speed from the same direction. (b) Two cars pass by from opposite directions. The star represents the LTE terminal.

where θ is the angle between the direction of car movement and the direction from the car to the LTE terminal, as shown in Figure 11 (a). λ is the wavelength of the received LTE signal. To estimate the Doppler shift from the received signal, we perform FFT on the phase variations received within one correlation window, *i.e.*, 0.2 second. We extract the highest peak on the spectrum whose frequency is the estimated Doppler shift f_s, as shown in Figure 10 (b). We know from Eq. 7 that, to calculate car speed v, we still need to know the θ, whose value, however, changes with the car movement as shown in Figure 11 (b). To accurately estimate the car speed in presence of the unknown time-varying θ, we propose a maximum likelihood estimator.

We assume that the speed of the car is a constant during a period of two seconds (a period of 10 correlation windows). Inside each correlation window, the car travels a distance of $\Delta l = vt$, where $t = 0.2\ s$ is the length of the window, as shown in Figure 11 (b). Supposing the horizontal and vertical distances between the car and the LTE terminal in the first window are l and d, respectively, we then obtain the angel θ_i of the i-th window as:

$$\theta_i = \arctan\left(\frac{d}{l-(i-1)vt}\right) \tag{8}$$

After obtaining θ, we calculate the theoretical Doppler shift vector $F(d,l,v)$ as:

$$F(d,l,v) = \begin{bmatrix} f_{s_1}(d,l,v) \\ f_{s_2}(d,l,v) \\ \cdots \\ f_{s_M}(d,l,v) \end{bmatrix} = \frac{v}{\lambda}\begin{bmatrix} \cos(\theta_1) \\ \cos(\theta_2) \\ \cdots \\ \cos(\theta_M) \end{bmatrix} \tag{9}$$

where $f_{s_i}(d,l,v)$ represents the Doppler shift introduced in the i-th window. On the other hand, we could estimate the Doppler shift

$$F' = \begin{bmatrix} f'_{s_1} & f'_{s_2} & \cdots & f'_{s_M} \end{bmatrix}^T \tag{10}$$

by performing FFT on the received phase variations. We then estimate the three unknown parameters d, l, and v by solving the maximum-likelihood problem below:

$$(d,l,v) = \arg\min \|F(d,l,v) - F'\| \tag{11}$$

We solve this maximum-likelihood problem using the Gurobi Library [15]. We update the estimation every two seconds.

6.2 Car counting

As the proposed system can detect the approaching of a car, naturally, our system can be utilized to count the number of cars passing by. In most cases, we can detect cars using the scheme introduced in Section 6.1. When there are two cars very close to each other as shown in Figure 12 (a) and (b), even if the two cars move at the same speed, they cause different Doppler frequency shifts because angle θ_1 is not equal to θ_2. Therefore, two prominent peaks will be shown on the spectrum plot, and we count them as two cars. Our current system targets at two-lane roads (one lane at each direction). We discuss the cases with more lanes in the discussion section.

Our system can also distinguish cars from other small objects such as bicycles and motorcycles on the road by signal strength. We observe that the signal reflections from cars are much stronger than those from bicycles and motorcycles, because a car is made of large pieces of metals and thus has much stronger RF reflections.

7 EVALUATION

In this section, we conduct experiments in different indoor and outdoor environments to evaluate the performance of LTE sensing.

7.1 Hardware implementation

We build a prototype receiver on an NI USRP B210 [29] which can be powered by a 5V USB power source (e.g., a laptop) or a portable power bank. It is suitable for both indoor and outdoor experiments. We use a Lenovo Thinkpad x1 carbon laptop (i7-8665U, 1.9GHz, 16GB RAM) for signal processing. For the software part, we modify the codes from srsLTE [32] (an open-source 4G structure project) to continuously extract LTE CSI, and process the received signals with MATLAB.

7.2 Evaluation of respiration sensing

In this section, we evaluate the performance of the proposed LTE-based pervasive respiration sensing system.

Experiment setup. We deploy the proposed respiration sensing system in two typical indoor environments, a small residential house and a large university office building that has over 50 rooms. We divide the whole residential house into two areas: *home living area* which includes the living room and three bedrooms, and *home corridor area* which includes the corridor and bathroom. We conduct experiments at 25 selected areas inside the office building. We classify the 25 areas into three categories: *office 1-wall area* that has one wall between the area and the outdoor, *office 2-wall area* that has two walls between the area and the outdoor, and *office 3-wall area* that has at least three walls between the area and the outdoor. Among the 25 selected areas, we have 12 office 1-wall areas, five 2-wall areas and eight 3-wall areas. Six volunteers are involved in the experiments, including two males and four females. As shown in Figure 8 (c) and (d), they are asked to sit during the experiments and change their orientations following our instructions. In total, we obtain more than 6000 records of one-minute human respiration trace in a period of half year. We use the Hexoskin Smart Garments [16] to measure the ground-truth respiration rate.

7.2.1 Coverage of LTE-based respiration sensing. We first investigate the coverage of our LTE-based respiration sensing system. In this experiment, we randomly choose 40 locations from the home living area and 20 locations from the home corridor area inside the residential house. We also choose 10 locations from each of the 25 areas inside the office building. We place the LTE terminal at each location and then let the volunteer sit 0.5 m away from the terminal.

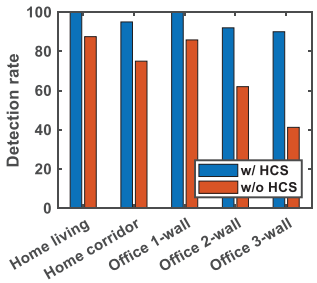

Figure 13: Overall detection rate at different types of areas. Performance comparison between with Heuristic Coordinate Shifting (HCS) and without HCS.

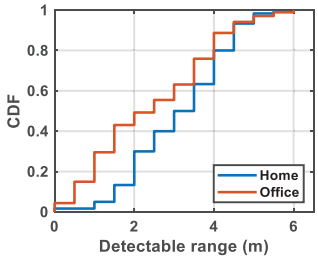

Figure 14: The CDF plot of maximum detectable receiver-target distance at different locations. "Detectable" means the average respiration rate error is less than 1 bpm.

We repeat the experiments 10 times at each location and compute the average respiration rate error. One location is considered as covered if the average respiration rate error is smaller than 1 *bpm*.

We calculate the coverage percentage as the ratio of the number of covered locations over the total number of locations and plot the results in different areas in Figure 13. We see from Figure 13 that the coverage percentages at different types of areas are always above 90% and the overall coverage is 95.4%. Specifically, we observe 100% coverage in the home living area and office 1-wall areas, which include bedrooms, living rooms and those office areas one wall from the outdoor. These areas are usually the places that need respiration rate monitoring most in real life. In home corridor area and office corridor areas, the coverage is slightly lower due to signal attenuation caused by walls. For those rooms deep inside the building, *i.e.*, with three walls between the area and the outdoor, the coverage is 90% which is still reasonably good. In comparison, the coverage for WiFi sensing in the office building is merely 15%.

We further evaluate the effectiveness of the proposed heuristic coordinate shifting scheme. Without heuristic coordinate shifting, the detection rates are decreased by 12.5%, 21%, 14.2%, 32.6% and 54.2% respectively. The results show that the proposed heuristic coordinate shifting scheme can help extract signal variation induced by target activities.

7.2.2 Receiver-target distance. For LTE sensing, the transmitter is far away from the target. We now evaluate the effect of distance between the receiver and target. We conduct experiments at the 310 locations selected in Section 7.2.1. We place an LTE terminal at the location and let the target move away at a step size of 0.5 m from the LTE terminal to measure the maximum distance between the target and LTE terminal that can still achieve a respiration rate estimation error less than 1 rpm. To reduce randomness, we repeat the experiment 10 times for each configuration and calculate the average error. We plot the CDF of measured maximum distances in the house and office building in Figure 14. We see that the mean detectable ranges in home and office are 3.1 m and 3.3 m, respectively.

To further demonstrate the relationship between the accuracy of LTE-based respiration rate estimation and the distance between the LTE terminal and the human target, we conduct an experiment in

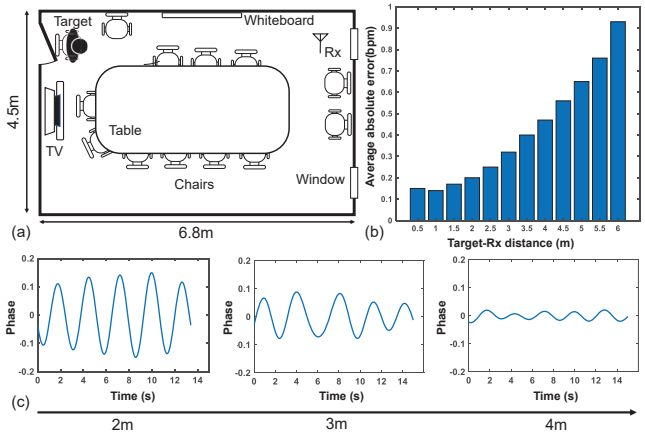

Figure 15: Experiment settings for accuracy vs. distance evaluation. (a) The layout of the conference room with furniture, target and receiver marked. (b) Mean error of respiration rate estimation versus distance to the LTE terminal. (c) Respiration patterns at three target locations with different distances to the LTE terminal.

a large conference room full of furniture as shown in Figure 15 (a), where the LTE terminal is placed close to the window, and the human target sits in a chair and breaths naturally. We let the target change locations and vary the distance from the receiver at a step size of 0.5 m. We use a laser distance meter [6] to measure the distance between the target chest and the LTE terminal.

Figure 15 (b) depicts the average absolute errors of the estimated respiration rate. When the target moves away from the LTE terminal, the average error increases. This is because the reflected signal from the target chest attenuates along the reflection path, causing a lower SNR and thus a larger estimation error. However, we want to point out that at a distance of 6 m, the error is still reasonably small at 0.93 rpm. To further demonstrate the impact of distance between the human target and LTE terminal, we also plot the extracted respiration pattern in Figure 15 (c). We could see that the pattern is much clearer when the distance is smaller. Generally, the respiration rate estimation error of 1 bpm is considered acceptable for real-life applications [46]. That is to say, the *target-device distance* of LTE-Track can be six meters, which is large enough to monitor human respiration in a room using an LTE-equipped device such as a smartphone or a smartwatch.

7.2.3 Impact of blind spot and target orientation. We evaluate the robustness of the proposed LTE sensing system against the blind spot issue and orientation issue. We place the LTE terminal at one position and then uniformly select 30 locations from the area within a radius of two meters from the terminal. We let the target sit at 30 locations and then estimate the target's respiration rate. At each location, we also let the target change his/her orientation by facing six different directions. For each combination of location and orientation, we repeat the experiment for 10 times. At each location, we check whether we can obtain a reliable respiration rate estimation with an error less than 1 bpm. We conduct experiments in a bedroom of the residential house and in two rooms of the office building, one *office 1-wall area* and one *office 3-wall area*.

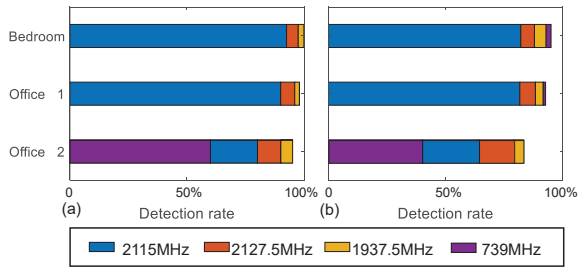

Figure 16: (a) The aggregated detection rate at different locations using information from multiple base stations with the target facing the LTE terminal. (b) The aggregated detection rate with both target location and orientation varied.

We calculate the detection rate as the ratio of the number of combinations (location, orientation) that we can obtain reliable respiration estimation over the total number of combinations. We plot the results in Figure 16, from which we could see that LTE-Track selects four base stations, *i.e.*, 2115 MHz, 2127.5 MHz, 1937.5 MHz and 739 MHz for respiration rate estimation in the three rooms. In Figure 16 (a), we plot the aggregated detection rate when the target is facing the LTE terminal. From left to right, we sort the base stations in the descending order based on the RSNR values. We aggregate information from multiple base stations to improve robustness. We can see that by aggregating information from four base stations, LTE-Track is able to cover 100%, 98% and 95% locations we have tested in the bedroom, office 1 and office 2, respectively. Note that for office 1, those locations covered by the 739 MHz base station are all covered by the other three base stations, that is, 739 MHz does not make additional contribution in office 1. Therefore, it is not plotted on the stacked bar. The ratio decreases to 93%, 90% and 60%, if we only use the single base station that has the strongest RSNR in the three rooms, causing significantly more blind spots. In summary, by utilizing the spatial diversity of multiple base stations, LTE-Track successfully reduces the number of blind spots in the three rooms by 70%, 80% and 87.5%, respectively.

To further investigate the impact of target orientation, we plot the average detection rate for six different directions at each location in Figure 16 (b). We could see that LTE-Track is able to cover 95%, 92% and 83% locations in the bedroom, office 1 and office 2, respectively. Note that for office 2 which is blocked by three walls from the outdoor, the sensing performance of every single base station is degraded. Even for the base station with the highest RSNR, the detection rate is just about 40%. By involving multiple base stations, we improve the detection rate by more than 100%. To summarize, orientation indeed affects the detection rate but LTE-Track still achieves robust performance across different orientations by fully utilizing the LTE frequency and spatial diversity.

7.2.4 Effect of weather and times of day. We observe that the LTE signal received is affected by times of day (*i.e.*, daytime or night) and weather. To quantify their impacts on respiration rate estimation, we conduct experiments with varying times of day and weather. In each experiment, we place the LTE terminal at the same location, and let the target face the LTE terminal. We estimate the respiration rate with a target sitting at 10 predetermined locations that have

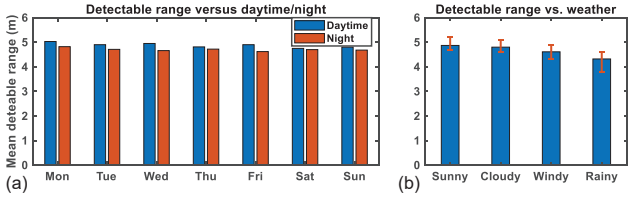

Figure 17: Impacts of times of day and weather on respiration sensing. *Detectable* means the respiration rate estimation error is smaller than 1 bpm.

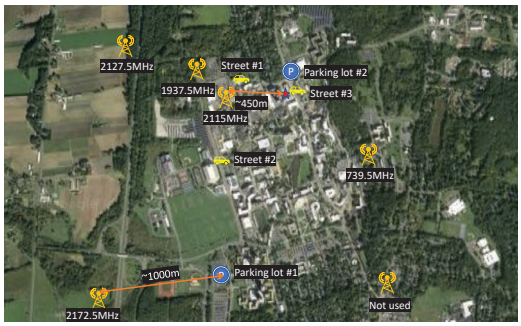

Figure 18: The distribution of LTE base stations and experiment sites. Orange towers denote the base stations, yellow cars denote the road experiment sites, red star denotes the office building and parking signs denote the parking lots.

varying distances with respect to the LTE terminal. We repeat the experiments 10 times for each configuration. Based on the estimation results at the 10 locations, we calculate the maximum target-receiver distance which can still maintain an error smaller than 1 bpm. To evaluate the effect of daytime and night, we repeat the experiment and record data for a week. To evaluate the effect of different weather conditions, we collect the data for one month, with 14 sunny days, five cloudy days, seven windy days and four rainy days. We plot the results in Figure 17. We could see from Figure 17 (a) that on average, the maximum target-receiver distance at night is 0.17 m shorter than that in daytime. A possible reason is that LTE base stations switch to power-saving mode [41] at night. The lower signal strength results in lower SNR and lower sensing capability. On the other hand, we could see from Figure 17 (b) that the weather has a noticeable impact on sensing performance. Specifically, the maximum target-receiver distance in rainy days is about one meter smaller than that in sunny days.

7.3 Evaluation of car speed estimation and counting

In this section, we evaluate the performance of our LTE-based car speed estimation and car counting system.

Methodology. We deploy our system at five different sites including two parking lots and three roads in our university, as shown in Figure 18. Two experiment scenarios are shown in Figure 19. In each scenario, we measure the speed of five different cars including two sedans and three SUVs. In the parking lots, we increase the car speed from 25 mph to 50 mph at a step size of 5 mph. Due to the

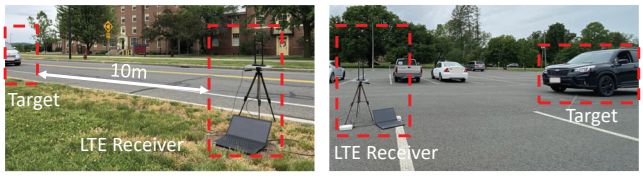

Figure 19: Experiment scenarios of car speed estimation. (a) Road scenario. (b) Parking lot scenario.

Table 1: Distance to base stations and corresponding signal strength.

(d, S), d is the site-BS distance in meter and S is signal strength in dB.				
Sites	2115 MHz	2127.5 MHz	1937.5 MHz	2172.5 MHz
Parking lot #1	(1262, -76)	–	–	(971,-69)
Street #1	(182, -59)	(978, -63)	(341, -64)	–
Street #2	(508, -65)	(1151, -68)	(794, -69)	–
Street #3	(519, -65)	(1312, -66)	(793, -71)	–
Parking lot #2	(497, -61)	(1189, -65)	(705, -69)	–

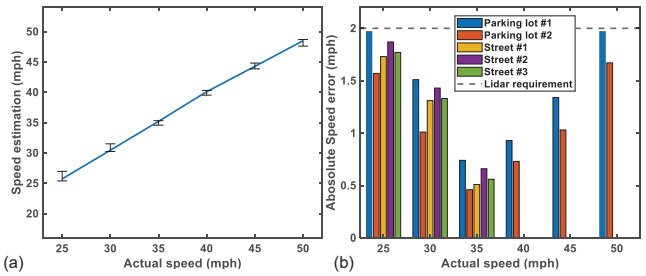

Figure 20: (a) Average speed estimation error versus the actual speed. (b) Average speed estimation error at different sites. The dot line indicates the accuracy requirement for Lidar.

speed limit, we only increase the speed from 25 mph to 35 mph for the three roads. We repeat each experiment for ten times. We use the cruise control during the experiment process and use the speed as the ground truth.

7.3.1 Accuracy of speed estimation. Figure 20 (a) shows both the average and 90% absolute error of the car speed estimation. We observe that from 25 mph to 35 mph, the speed error decreases, while the speed error increases from 35 mph to 50 mph. We believe the increasing accuracy when we first increase the speed is because a larger Doppler shift can be measured more accurately. However, when we further increase the speed, the 1000 Hz sampling rate becomes the bottleneck for sensing. We plan to utilize higher frequency sampling rate leveraging the LTE OFDM symbols (14 OFDM symbols per subframe) in the future for higher speed monitoring.

Figure 20 (b) shows the average speed error across multiple locations marked on the map in Figure 18. The corresponding signal strengths from different base stations are shown in Table 1. We choose the base station with the highest signal strength for sensing, which is 2172.5 MHz for Parking lot #1 and 2115 MHz for the other locations. We observe lower speed estimation error in Parking lot #2 compared with other locations. The main reason is that Parking

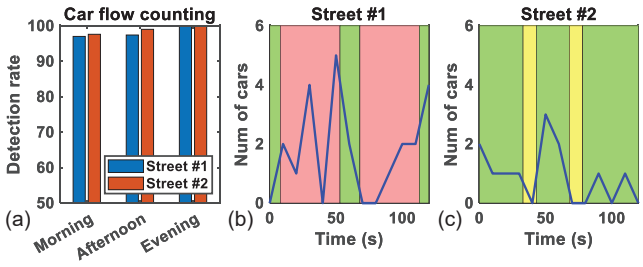

Figure 21: (a) Detection rate of car counting in a day. (b) A 120-s record of the car flow on street #2. Each data point represents the aggregated number of cars in a window of 10 s. (c) A 120-s record of the car flow on street #1.

lot #2 is close to a base station (497 m) and therefore has a high signal strength (-61 dBm). On the other hand, Street #1 is closer to one base station (182 m) but it shows higher speed error. We believe this is because there exists interference from nearby woods and buildings. The results at other locations are consistent with the received signal strengths and their distances to the base stations. Generally speaking, smaller distance and higher signal strength improve the speed estimation accuracy. The average speed error for all the locations is lower than 2 mph which satisfies the accuracy requirement for commodity car speed measurement device [4].

7.3.2 Accuracy of car counting. We conduct experiments to count the number of cars passing by on two two-lane roads (one line per direction) in the university. Specifically, we place the LTE terminal near the traffic light at Street #2, and near a pedestrian crossing button at Street #1. At each location, we record signal traces for two hours and collect the ground truth of passing cars using a camera.

We compute the detection rate as the number of detected cars over the total number of cars and plot the results in Figure 21 (a). We see that the detection rate is always higher than 95% across location and time, demonstrating the robustness of LTE-Track. We also plot the variation of the number of detected cars over time in Figure 21 (b) and (c), from which we see that Street #2 is busier than Street #1. From Figure 21 (b), we see that 12 cars pass by the LTE terminal in the first period of red light (red background color). In Figure 21 (c), when pedestrians are crossing the street (crossing button pressed, yellow background color), the car flow is stopped and we see two clear breaks in the figure. The car flow information can help the traffic system to adjust the waiting time of the crossing button to balance the car flow and pedestrian flow.

8 RELATED WORK

LTE sensing. Existing LTE-based works for passive sensing mainly focus on fingerprint-based localization [26, 27, 51] by collecting CSI measurements at different locations and build up a database to achieve coarse localization in both indoor and outdoor scenarios. Similarly, some works [5, 30, 31] collect the reflected CSI from passing cars to build up a fingerprint database for car type classification. A recent work [10] further utilizes LTE signals for fine-grained hand gesture recognition under the premise that a strong line-of-sight path exists from the base station to the receiver, while our

work realizes fine-grained sensing in non-light-of-sight environments with interference and noise. SpiderMon [22] is an LTE-based system on keystroke sensing. While SpiderMon does not work with omnidirectional antennas, the authors utilize a high-gain (24 dBi) parabolic antenna to achieve keystroke sensing. In comparison, we achieve fine-grained sensing using omnidirectional antennas.

Respiration sensing. Respiration sensing is a popular area in wireless sensing and mobile health. WiFi-based respiration sensing has attracted a huge amount of attention. Wi-Sleep [23] is a pioneer work on WiFi-based respiration sensing. To improve the respiration sensing performance, Niu et al. [25] introduce a method of adding virtual multipath to the original signal to boost the signal variation to improve the sensing performance. On the other hand, Fresnel zone theories [36, 50] are proposed to explain the underlying mechanism behind the *blind spot* and orientation-sensitive issues. PhaseBeat [39] leverage the phase difference of two antennas connected to the same WiFi AP to extract respiration pattern. FarSense [47] leverages the CSI ratio and further combines the amplitude and phase information to increase the sensing range. People also exploit diverse techniques such as UWB [19, 34], FMCW [3] and LoRa [42, 48] for respiration sensing. These technologies require dedicate hardware which is not available in most environments. Furthermore, all existing wireless sensing systems require the target to be located near to the transmitter, while in our system, the target can be hundreds and even thousands of meters away from the LTE base stations. Given the extensive deployment of LTE infrastructure, we are able to achieve a more pervasive coverage.

Car speed estimation and counting. Car counting and speed estimation are key components of traffic monitoring. Researchers propose low-cost customized devices [1] to replace expensive commercial equipment. The key idea is to communicate with the ETC (Electronic Toll Collection) RFID tag attached to a car, using their customized RFID reader. The key difference between the existing design [1] and our proposed solution is that the existing design requires every car to be equipped with an RFID tag in order to be sensed, while our solution does not require any dedicated hardware to be installed on the car. Furthermore, the solution proposed in [1] requires two RFID readers separated by a known distance to be deployed along the road, while our solution only requires one LTE terminal to achieve almost instantaneous speed estimation.

9 DISCUSSION

Comparison with WiFi-based "pervasive" sensing. It is hard to conduct an absolute fair comparison between WiFi-based and LTE-based sensing solutions, since LTE base stations are often hundreds of times further away from the target compared to WiFi APs. We compare the proposed system with FarSense, the state-of-art long-range WiFi respiration sensing system [47]. In terms of accuracy, results show that FarSense achieves an error of 0.34 bpm when the transmitter is 5 m away in another room and the receiver is 1 m away in the same room. Our experiments show an error of 0.14 bpm when the receiver is 1 m away from the target and the base stations are at least 400 meters away. In terms of sensing coverage, FarSense covers a range of eight meters in LOS scenarios and five meteres in NLOS scenarios around the transmitter. The WiFi sensing coverage is about 15% in our office building. In comparison, LTE sensing can achieve over 90% coverage in the same office building.

Multi-target respiration sensing. When there are multiple targets, the reflection signals get mixed together at the receiver, and it is challenging to separate them to sense each individual. Separating signals spatially requires the LTE terminal to be equipped with an antenna array which is currently not available at most commodity LTE devices. One potential solution is to only amplify the signal variation induced by one target within a specified zone while suppressing the signal variation induced by other targets. However, this method still requires the targets to be sparsely located.

Multi-lane scenario in car counting. For a wide road with multiple lanes in one direction, multiple cars may approach the LTE terminal side by side. In this case, the signals reflected from multiple cars can be mixed at the receiver. We need to separate the signals before we can obtain the information of each car. We believe we can utilize LTE-Advanced devices with more antennas and adopt multi-dimensional signal separation method proposed in mD-Track [44] to enable simultaneous multi-car tracking.

LTE picocells for indoor environment. In recent years, there are more and more LTE picocells deployed to enhance indoor LTE communication. With the benefit of stronger signals and less interference, we believe LTE picocells favor our design and the proposed system would perform better.

Limitations. Although the proposed system achieves more than 90% coverage in an office building with complicated structures, there are still blind spots such as bathrooms blocked by four or five walls. With the growing deployment of metrocells, picocells and femtocells, we believe the blind spot issue will be further mitigated. Another limitation is that while we successfully demonstrate the feasibility of LTE sensing using a software-defined radio platform as the receiver, it is still challenging for us to retrieve LTE CSI readings from commodity devices such as a smartphone.

10 CONCLUSION

In this paper, we for the first time analyze the unique features and advantages of LTE sensing. We demonstrate the superior performance of LTE sensing in terms of sensing coverage and robustness using two typical applications, indoor respiration sensing and outdoor traffic monitoring. We believe LTE-Track moves a big step towards truly pervasive sensing and presents a new sensing modality on LTE devices.

ACKNOWLEDGEMENTS

The research reported in this paper was sponsored in part by the CCDC Army Research Laboratory (ARL) under Cooperative Agreement W911NF-17-2-0196 (ARL IoBT CRA), and supported by UMass Amherst Institute for Applied Life Sciences (IALS) Equipment Fund. The views and conclusions contained in this document are those of the authors and should not be interpreted as representing the official policies, either expressed or implied, of the ARL, NSF or the U.S. Government. The U.S. Government is authorized to reproduce and distribute reprints for Government purposes notwithstanding any copyright notation herein.

REFERENCES

[1] Omid Abari, Deepak Vasisht, Dina Katabi, and Anantha Chandrakasan. 2015. Caraoke: An E-Toll Transponder Network for Smart Cities. *SIGCOMM Comput. Commun. Rev.* 45, 4 (Aug. 2015), 297–310. https://doi.org/10.1145/2829988.2787504

[2] Heba Abdelnasser, Moustafa Youssef, and Khaled A. Harras. 2015. WiGest: A ubiquitous WiFi-based gesture recognition system. In *2015 IEEE Conference on Computer Communications (INFOCOM)*. IEEE, 1472–1480. https://doi.org/10.1109/INFOCOM.2015.7218525

[3] Fadel Adib, Hongzi Mao, Zachary Kabelac, Dina Katabi, and Robert C. Miller. 2015. Smart Homes That Monitor Breathing and Heart Rate. In *Proceedings of the 33rd Annual ACM Conference on Human Factors in Computing Systems* (Seoul, Republic of Korea) *(CHI '15)*. Association for Computing Machinery, New York, NY, USA, 837–846. https://doi.org/10.1145/2702123.2702200

[4] National Highway Traffic Safety Administration. 2013. *NHTSA lidar specifications. https://www.nhtsa.gov/staticfiles/nti/pdf/809811-LIDARSpeedMeasuringDevice.pdf.* U.S. Department of Transportation.

[5] Nadia Adnan Shiltagh Al-Jamali and Hamed S Al-Raweshidy. 2021. Smart IoT Network Based Convolutional Recurrent Neural Network With Element-Wise Prediction System. *IEEE Access* 9 (2021), 47864–47874.

[6] AVIDPOWER. 2021. *Laser Distance Measure. https://avidpowertool.com/collections/measure-test/products/laser-distance-measure-229ft-m-in-ft-digital-laser-meter-with-mute-function-2-bubble-levels-backlit-lcd-and-pythagorean-mode-measure-distance-area-and-volume-battery-included.* AVIDPOWER.

[7] John J Benedetto. 1993. *Wavelets: mathematics and applications*. Vol. 13. CRC press.

[8] Police Radar Information Center. 2017. *Speed Radar Test and Calibration. https://copradar.com/chapts/chapt3/ch3d4.html.* Police Radar Information Center.

[9] Baicheng Chen, Huining Li, Zhengxiong Li, Xingyu Chen, Chenhan Xu, and Wenyao Xu. 2020. ThermoWave: A New Paradigm of Wireless Passive Temperature Monitoring via MmWave Sensing. In *Proceedings of the 26th Annual International Conference on Mobile Computing and Networking* (London, United Kingdom) *(MobiCom '20)*. Association for Computing Machinery, New York, NY, USA, Article 27, 14 pages. https://doi.org/10.1145/3372224.3419184

[10] Weiyan Chen, Kai Niu, Deng Zhao, Rong Zheng, Dan Wu, Wei Wang, Leye Wang, and Daqing Zhang. 2020. Robust dynamic hand gesture interaction using LTE terminals. In *2020 19th ACM/IEEE International Conference on Information Processing in Sensor Networks (IPSN)*. IEEE, 109–120.

[11] Federal Communications Commission. 2020. *2020 COMMUNICATIONS MARKETPLACE REPORT. https://docs.fcc.gov/public/attachments/FCC-20-188A1.pdf.* Federal Communications Commission.

[12] Wikipedia contributors. 2021. *Fading. https://en.wikipedia.org/wiki/Fading#cite_note-1.* Wikipedia.

[13] Wikipedia contributors. 2021. *Gradient descent. https://en.wikipedia.org/wiki/Gradient_descent.* Wikipedia.

[14] LTE Encyclopedia. 2021. *LTE Radio Link Budgeting and RF Planning. https://sites.google.com/site/lteencyclopedia/lte-radio-link-budgeting-and-rf-planning.* LTE Encyclopedia.

[15] LLC Gurobi Optimization. 2021. LLC Gurobi Optimization. Video. https://www.gurobi.com/products/gurobi-optimizer/

[16] Carre Technologies inc. 2021. *Hexoskin Smart Garments. https://www.hexoskin.com/.* Carre Technologies inc.

[17] Mona Jaber, Zaher Dawy, Naeem Akl, and Elias Yaacoub. 2015. Tutorial on LTE/LTE-A cellular network dimensioning using iterative statistical analysis. *IEEE Communications Surveys & Tutorials* 18, 2 (2015), 1355–1383.

[18] Chengkun Jiang, Junchen Guo, Yuan He, Meng Jin, Shuai Li, and Yunhao Liu. 2020. mmVib: micrometer-level vibration measurement with mmwave radar. In *Proceedings of the 26th Annual International Conference on Mobile Computing and Networking*. 1–13.

[19] Joshua Chong Yue Lai, Ying Xu, Erry Gunawan, Eric Chern-Pin Chua, Arash Maskooki, Yong Liang Guan, Kay-Soon Low, Cheong Boon Soh, and Chueh-Loo Poh. 2010. Wireless sensing of human respiratory parameters by low-power ultrawideband impulse radio radar. *IEEE Transactions on Instrumentation and Measurement* 60, 3 (2010), 928–938.

[20] Yan Li and Ting Zhu. 2016. Gait-Based Wi-Fi Signatures for Privacy-Preserving. In *Proceedings of the 11th ACM on Asia Conference on Computer and Communications Security* (Xi'an, China) *(ASIA CCS '16)*. Association for Computing Machinery, New York, NY, USA, 571–582. https://doi.org/10.1145/2897845.2897909

[21] Olof Liberg, Marten Sundberg, Eric Wang, Johan Bergman, and Joachim Sachs. 2017. *Cellular Internet of things: technologies, standards, and performance*. Academic Press.

[22] Kang Ling, Yuntang Liu, Ke Sun, Wei Wang, Lei Xie, and Qing Gu. 2020. SpiderMon: Towards Using Cell Towers as Illuminating Sources for Keystroke Monitoring. In *IEEE INFOCOM 2020 - IEEE Conference on Computer Communications*. 666–675. https://doi.org/10.1109/INFOCOM41043.2020.9155447

[23] Xuefeng Liu, Jiannong Cao, Shaojie Tang, and Jiaqi Wen. 2014. Wi-sleep: Contactless sleep monitoring via wifi signals. In *2014 IEEE Real-Time Systems Symposium*. IEEE, IEEE, 346–355.

[24] Kai Niu, Fusang Zhang, Xuanzhi Wang, Qin Lv, Haitong Luo, and Daqing Zhang. 2021. Understanding WiFi Signal Frequency Features for Position-Independent Gesture Sensing. *IEEE Transactions on Mobile Computing* (2021), 1–1. https://doi.org/10.1109/TMC.2021.3063135

[25] Kai Niu, Fusang Zhang, Jie Xiong, Xiang Li, Enze Yi, and Daqing Zhang. 2018. Boosting Fine-Grained Activity Sensing by Embracing Wireless Multipath Effects. In *Proceedings of the 14th International Conference on Emerging Networking EXperiments and Technologies* (Heraklion, Greece) *(CoNEXT '18)*. Association for Computing Machinery, New York, NY, USA, 139–151. https://doi.org/10.1145/3281411.3281425

[26] Giovanni Pecoraro, Ernestina Cianca, Simone Di Domenico, and Mauro De Sanctis. 2018. LTE Signal Fingerprinting Device-Free Passive Localization Robust to Environment Changes. In *2018 Global Wireless Summit (GWS)*. IEEE, 114–118.

[27] Giovanni Pecoraro, Simone Di Domenico, Ernestina Cianca, and Mauro De Sanctis. 2017. LTE signal fingerprinting localization based on CSI. In *2017 IEEE 13th International Conference on Wireless and Mobile Computing, Networking and Communications (WiMob)*. IEEE, 1–8.

[28] Kun Qian, Chenshu Wu, Zheng Yang, Yunhao Liu, and Kyle Jamieson. 2017. Widar: Decimeter-Level Passive Tracking via Velocity Monitoring with Commodity Wi-Fi. In *Proceedings of the 18th ACM International Symposium on Mobile Ad Hoc Networking and Computing* (Chennai, India) *(Mobihoc '17)*. Association for Computing Machinery, New York, NY, USA, Article 6, 10 pages. https://doi.org/10.1145/3084041.3084067

[29] Ettus Research. 2021. *USRP B210. https://www.ettus.com/all-products/ub210-kit/.* Ettus Research.

[30] Santu Sardar, Amit K Mishra, and Mohammed Zafar Ali Khan. 2019. CommSense: a communication infrastructure based sensing instrument for environment monitoring. *CSI Transactions on ICT* 7, 2 (2019), 71–74.

[31] Santu Sardar, Amit K Mishra, and Mohammed Zafar Ali Khan. 2019. Vehicle detection and classification using LTE-CommSense. *IET Radar, Sonar & Navigation* 13, 5 (2019), 850–857.

[32] Software Radio Systems. 2021. *srsran. https://www.srsran.com/.* Software Radio Systems.

[33] Sheng Tan and Jie Yang. 2016. WiFinger: Leveraging Commodity WiFi for Fine-Grained Finger Gesture Recognition. In *Proceedings of the 17th ACM International Symposium on Mobile Ad Hoc Networking and Computing* (Paderborn, Germany) *(MobiHoc '16)*. Association for Computing Machinery, New York, NY, USA, 201–210. https://doi.org/10.1145/2942358.2942393

[34] Swaroop Venkatesh, Christopher R Anderson, Natalia V Rivera, and R Michael Buehrer. 2005. Implementation and analysis of respiration-rate estimation using impulse-based UWB. In *MILCOM 2005-2005 IEEE Military Communications Conference*. IEEE, IEEE, 3314–3320.

[35] Aditya Virmani and Muhammad Shahzad. 2017. Position and Orientation Agnostic Gesture Recognition Using WiFi. In *Proceedings of the 15th Annual International Conference on Mobile Systems, Applications, and Services* (Niagara Falls, New York, USA) *(MobiSys '17)*. Association for Computing Machinery, New York, NY, USA, 252–264. https://doi.org/10.1145/3081333.3081340

[36] Hao Wang, Daqing Zhang, Junyi Ma, Yasha Wang, Yuxiang Wang, Dan Wu, Tao Gu, and Bing Xie. 2016. Human respiration detection with commodity wifi devices: do user location and body orientation matter?. In *Proceedings of the 2016 ACM International Joint Conference on Pervasive and Ubiquitous Computing*. 25–36.

[37] Wei Wang, Alex X. Liu, and Muhammad Shahzad. 2016. Gait Recognition Using Wifi Signals. In *Proceedings of the 2016 ACM International Joint Conference on Pervasive and Ubiquitous Computing* (Heidelberg, Germany) *(UbiComp '16)*. Association for Computing Machinery, New York, NY, USA, 363–373. https://doi.org/10.1145/2971648.2971670

[38] Wei Wang, Alex X Liu, Muhammad Shahzad, Kang Ling, and Sanglu Lu. 2015. Understanding and modeling of wifi signal based human activity recognition. In *Proceedings of the 21st annual international conference on mobile computing and networking*. 65–76.

[39] Xuyu Wang, Chao Yang, and Shiwen Mao. 2017. PhaseBeat: Exploiting CSI phase data for vital sign monitoring with commodity WiFi devices. In *2017 IEEE 37th International Conference on Distributed Computing Systems (ICDCS)*. IEEE, 1230–1239.

[40] Chenshu Wu, Feng Zhang, Yuqian Hu, and K. J. Ray Liu. 2021. GaitWay: Monitoring and Recognizing Gait Speed Through the Walls. *IEEE Transactions on Mobile Computing* 20, 6 (2021), 2186–2199. https://doi.org/10.1109/TMC.2020.2975158

[41] Jingjin Wu, Yujing Zhang, Moshe Zukerman, and Edward Kai-Ning Yung. 2015. Energy-efficient base-stations sleep-mode techniques in green cellular networks: A survey. *IEEE communications surveys & tutorials* 17, 2 (2015), 803–826.

[42] Binbin Xie and Jie Xiong. 2020. Combating Interference for Long Range LoRa Sensing. In *Proceedings of the 18th Conference on Embedded Networked Sensor Systems* (Virtual Event, Japan) *(SenSys '20)*. Association for Computing Machinery, New York, NY, USA, 69–81. https://doi.org/10.1145/3384419.3430731

[43] Binbin Xie, Yuqing Yin, and Jie Xiong. 2021. Pushing the Limits of Long Range Wireless Sensing with LoRa. *Proc. ACM Interact. Mob. Wearable Ubiquitous Technol.* 5, 3, Article 134 (Sept. 2021), 21 pages. https://doi.org/10.1145/3478080

[44] Yaxiong Xie, Jie Xiong, Mo Li, and Kyle Jamieson. 2019. MD-Track: Leveraging Multi-Dimensionality for Passive Indoor Wi-Fi Tracking. In *The 25th Annual International Conference on Mobile Computing and Networking* (Los Cabos, Mexico) *(MobiCom '19)*. Association for Computing Machinery, New York, NY, USA, Article 8, 16 pages. https://doi.org/10.1145/3300061.3300133

[45] Lei Yang, Yao Li, Qiongzheng Lin, Xiang-Yang Li, and Yunhao Liu. 2016. Making Sense of Mechanical Vibration Period with Sub-Millisecond Accuracy Using Backscatter Signals. In *Proceedings of the 22nd Annual International Conference on Mobile Computing and Networking* (New York City, New York) *(MobiCom '16)*. Association for Computing Machinery, New York, NY, USA, 16–28. https://doi.org/10.1145/2973750.2973759

[46] Youwei Zeng, Dan Wu, Jie Xiong, Jinyi Liu, Zhaopeng Liu, and Daqing Zhang. 2020. MultiSense: Enabling multi-person respiration sensing with commodity wifi. *Proceedings of the ACM on Interactive, Mobile, Wearable and Ubiquitous Technologies* 4, 3 (2020), 1–29.

[47] Youwei Zeng, Dan Wu, Jie Xiong, Enze Yi, Ruiyang Gao, and Daqing Zhang. 2019. FarSense: Pushing the range limit of WiFi-based respiration sensing with CSI ratio of two antennas. *Proceedings of the ACM on Interactive, Mobile, Wearable and Ubiquitous Technologies* 3, 3 (2019), 1–26.

[48] Fusang Zhang, Zhaoxin Chang, Kai Niu, Jie Xiong, Beihong Jin, Qin Lv, and Daqing Zhang. 2020. Exploring lora for long-range through-wall sensing. *Proceedings of the ACM on Interactive, Mobile, Wearable and Ubiquitous Technologies* 4, 2 (2020), 1–27.

[49] Fusang Zhang, Zhaoxin Chang, Jie Xiong, Rong Zheng, Junqi Ma, Kai Niu, Beihong Jin, and Daqing Zhang. 2021. Unlocking the Beamforming Potential of LoRa for Long-Range Multi-Target Respiration Sensing. *Proc. ACM Interact. Mob. Wearable Ubiquitous Technol.* 5, 2, Article 85 (June 2021), 25 pages. https://doi.org/10.1145/3463526

[50] Fusang Zhang, Daqing Zhang, Jie Xiong, Hao Wang, Kai Niu, Beihong Jin, and Yuxiang Wang. 2018. From Fresnel Diffraction Model to Fine-Grained Human Respiration Sensing with Commodity Wi-Fi Devices. *Proc. ACM Interact. Mob. Wearable Ubiquitous Technol.* 2, 1, Article 53 (March 2018), 23 pages. https://doi.org/10.1145/3191785

[51] Heng Zhang, Zhichao Zhang, Shunqing Zhang, Shugong Xu, and Shan Cao. 2019. Fingerprint-based localization using commercial LTE signals: A field-trial study. In *2019 IEEE 90th Vehicular Technology Conference (VTC2019-Fall)*. IEEE, 1–5.

[52] Yue Zheng, Yi Zhang, Kun Qian, Guidong Zhang, Yunhao Liu, Chenshu Wu, and Zheng Yang. 2019. Zero-Effort Cross-Domain Gesture Recognition with Wi-Fi. In *Proceedings of the 17th Annual International Conference on Mobile Systems, Applications, and Services* (Seoul, Republic of Korea) *(MobiSys '19)*. Association for Computing Machinery, New York, NY, USA, 313–325. https://doi.org/10.1145/3307334.3326081